Cell, Vol. 86, 159–171, July 12, 1996, Copyright ©1996 by Cell Press

Atm-Deficient Mice: A Paradigm of Ataxia Telangiectasia

Carrolee Barlow,* Shinji Hirotsune,* Richard Paylor,§ Marek Liyanage,‡ Michael Eckhaus,‖ Francis Collins,† Yosef Shiloh,# Jacqueline N. Crawley,§ Thomas Ried,‡ Danilo Tagle,† and Anthony Wynshaw-Boris*
*Laboratory of Genetic Disease Research
†Laboratory of Gene Transfer
‡Diagnostic Development Branch
National Center for Human Genome Research
§Section on Behavioral Neuropharmacology
Experimental Therapeutics Branch
National Institute of Mental Health
‖Veterinary Resources Program
National Center for Research Resources
National Institutes of Health
Bethesda, Maryland 20892
#Department of Human Genetics
Sackler School of Medicine
Tel Aviv University
Ramat Aviv 69978
Israel

Summary

A murine model of ataxia telangiectasia was created by disrupting the *Atm* locus via gene targeting. Mice homozygous for the disrupted *Atm* allele displayed growth retardation, neurologic dysfunction, male and female infertility secondary to the absence of mature gametes, defects in T lymphocyte maturation, and extreme sensitivity to γ-irradiation. The majority of animals developed malignant thymic lymphomas between 2 and 4 months of age. Several chromosomal anomalies were detected in one of these tumors. Fibroblasts from these mice grew slowly and exhibited abnormal radiation-induced G1 checkpoint function. *Atm*-disrupted mice recapitulate the ataxia telangiectasia phenotype in humans, providing a mammalian model in which to study the pathophysiology of this pleiotropic disorder.

Introduction

Ataxia telangiectasia (AT) is a human autosomal recessive disorder with a wide variety of clinical manifestations (Boder, 1975; Sedgewick and Boder, 1991). The hallmarks of AT are progressive neurologic degeneration, manifest mainly as cerebellar ataxia, choreoathetosis, and oculomotor dysfunction; oculocutaneous telangiectasias; recurrent sinopulmonary infections secondary to immunodeficiency; lymphoreticular malignancies; growth retardation; incomplete sexual maturation; endocrine abnormalities; and premature aging of the skin and hair. Individuals with AT are extremely sensitive to the effects of ionizing radiation. The disease is progressive and death generally occurs by the second or third decade of life owing to neurologic deterioration or lymphoreticular malignancies, which occur in about 10%–15% of patients (Taylor et al., 1996). No effective treatments have been found to alter the course of this disease. The frequency of AT in the United States and Britain has been estimated to be between 1:40,000 and 1:100,000, resulting in a carrier frequency of 0.5%–1.0%. Heterozygous carriers may also have a predisposition to cancer, particularly breast cancer (reviewed by Easton, 1994).

Pathologic analysis at autopsy demonstrates that AT is a systemic disorder (Boder, 1975; Sedgewick and Boder, 1991). Brains from patients with AT show neurodegenerative changes, particularly in the Purkinje and granular cells of the cerebellum. Neuronal degeneration is also present in the brainstem, dorsal root ganglia, spinal cord, and peripheral nerves. Immunodeficiency correlates with absent or hypoplastic thymus and hypoplasia of other lymphoid tissues. Gonadal abnormalities, particularly hypoplasia with germ cell deficiencies, are often seen postmortem. Thus, AT is a disorder with pleiotropic effects in postmitotic, mitotic, and meiotically active tissues.

Mitotic cells from AT patients, such as fibroblasts and lymphoblastoid lines, have a variety of characteristic anomalies in culture, including sensitivity to ionizing radiation and radiomimetic drugs, radioresistant DNA synthesis (RDS), chromosomal instability, reduced lifespan in culture, and high serum requirements (reviewed by Meyn, 1995; Shiloh, 1995). Although the kinetics of double-stranded break (DSB) repair is unaltered in AT cells, the radiosensitivity and chromosomal instability suggest a defect in the repair of particular types of DSBs. This is supported by studies in AT cells that demonstrate the presence of elevated levels of unrepaired DSBs in untreated and irradiated cells (Blocher et al., 1991; Coquerelle et al., 1987), abnormal rejoining of DSBs in plasmid-based recombination assays (Cox et al., 1986; Powell et al., 1993), and elevated levels of DSB conversion to chromosomal breaks (Liu and Bryant, 1994; Pandita and Hittelman, 1992a, 1992b). In addition to abnormalities in DSB repair, radiation-induced G1, S, and G2 checkpoints appear to function abnormally in AT cells (for review see Meyn, 1995; Shiloh, 1995). As a result, AT cells are defective in the postirradiation induction of p53 protein levels and *gadd45* (Artuso et al., 1995; Kastan et al., 1992). Thus, the gene product defective in AT appears to be important for DSB repair and is likely part of a signal transduction cascade regulating cell cycle progression after DNA damage.

AT was mapped to human 11q22-23 (Gatti et al., 1988), and the responsible gene (designated *ATM*, for AT mutated) was defined by positional cloning (Savitsky et al., 1995a, 1995b). The gene is approximately 150 kb in length, spread over 66 exons (Uziel et al., 1996). A 13 kb mRNA transcript contains an open reading frame of 9168 bp encoding a 350 kDa nuclear protein (K. Brown, F. C., and D. T., submitted). Mutations have been detected in over 100 AT patients, and more than 80% result in ATM protein truncations (Byrd et al., 1996; Gilad et al., 1996). The phenotype is similar in all patients, including those in which deletion of 90% of the gene has occurred, suggesting that all mutations are functionally equivalent

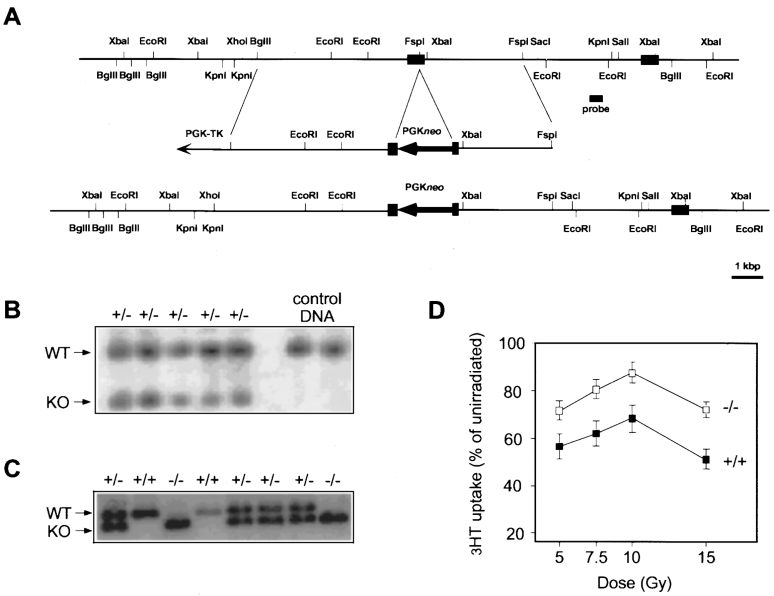

Figure 1. Generation of *Atm*-Disrupted Mice

Shown in (A) are the genomic locus surrounding the targeted exon, the targeting vector, and the targeted locus. Using the targeting vector, five independent embryonic stem cell clones were obtained. Southern blots of genomic DNA from correctly targeted (+/−) and control embryonic stem cells clones digested with XhoI (B) and one litter from a heterozygous cross digested with EcoRV (C). WT indicates wild-type locus and KO the targeted locus (B). (D) shows a graphic representation of RDS in *Atm*-disrupted fibroblasts as compared with fibroblasts from wild-type littermates ($p < 0.03$).

loss-of-function or null alleles. The mouse homolog, *Atm*, has also been identified (Pecker et al., 1996) and mapped to mouse chromosome 9C, which is syntenic to human 11q22-23. Atm shows 84% amino acid identity and 91% similarity with ATM. Sequence comparisons revealed that *ATM* and *Atm* are members of a family of genes involved in cell cycle regulation (*TOR1*, *TOR2*, and *MEC1* of Saccharomyces cerevisiae and *rad3* of Schizosaccharomyces pombe), telomere length monitoring (*TEL1* of S. cerevisiae), meiotic recombination (*MEC1* of S. cerevisiae and *mei41* of Drosophila melanogaster), and DNA repair (*DNA-PK*$_{CS}$) (reviewed by Zakian, 1995), supporting a role for *ATM* in DSB repair and cell cycle control.

Although it is possible to study the potential role of ATM in cell cycle regulation using invertebrate models, an understanding of the pleiotropic function of ATM inferred from the AT phenotype can be best studied in a mammalian model. We have created a mouse model of AT by disrupting the murine *Atm* locus by gene targeting and have characterized the phenotype of these mice. We have found that the phenotype of mice homozygous for the disruption of *Atm* is remarkably similar to the human AT phenotype.

Results

Creation of *Atm*-Disrupted Mice

To inactivate *Atm*, we introduced a truncation mutation into the gene at a position corresponding to the approximate location of at least ten protein truncation mutations found in individuals with AT (between nucleotides 5178–5979 of human *ATM*) (Savitsky et al., 1995b). A 178 bp exon, corresponding to nucleotides 5705–5882 in *Atm* (Pecker et al., 1996), was identified, sequenced, and disrupted (Figure 1A) by placing a PGK*neo* gene at position 5790 in the opposite orientation relative to *Atm* transcription. An *Atm* transcript including this modified exon would result in the truncation of the protein in the *neo* gene, and an *Atm* transcript that spliced around this modified exon would result in a frameshift and protein truncation. This targeted modification of *Atm* should be similar to several mutations of *ATM* in AT patients.

The *Atm*-targeting construct was transfected into TC1 embryonic stem cells (Deng et al., 1996), and targeted clones were selected (Figure 1B). Targeted clones were injected into blastocysts, and one clone transmitted the disrupted *Atm* allele (*Atm*^{ins5790neo}) in the germline of the mouse. Animals with an inbred or a mixed background were generated by mating chimeras with either 129/SvEv or NIH Black Swiss mice, respectively. No phenotypic variance was detected between the mixed and inbred backgrounds, and unless otherwise noted, no distinction was made during analysis.

F1 heterozygous offspring were inter-crossed, and F2 offspring were genotyped by Southern blot analysis. All three genotypes were detected in F2 litters (Figure 1C). Cumulative genotyping of heterozygous crosses revealed that the ratios of wild-type:heterozygote:homozygote mutant mice were 53:122:53 (1:2.3:1) in matings of mice with mixed background and 11:35:13 (1:3.2:1.2) in matings of completely inbred 129/SvEv mice. These ratios are not statistically different ($p > 0.3$ by chi-squared analysis) from the expected 1:2:1 Mendelian ratio. Thus, mice with a disruption of *Atm* are viable, as is the case in human AT.

Cell Cycle Checkpoint Abnormalities in Mutant Fibroblasts

We tested several antibodies to various regions of ATM on mouse tissues and cell lines by immunoblot analysis and have not found a cross-reacting antibody to Atm (K. Brown and D. T., unpublished data). Therefore, we determined the effectiveness of our knockout by an *Atm* functional assay in cells from mutant and wild-type mice. Cells from AT patients have abnormal cell cycle checkpoints after γ-irradiation (reviewed by Meyn, 1995; Shiloh, 1995). To determine whether cells from mice homozygous for the *Atm* disruption also had abnormal G1 checkpoint function, we examined RDS in tail fibroblasts

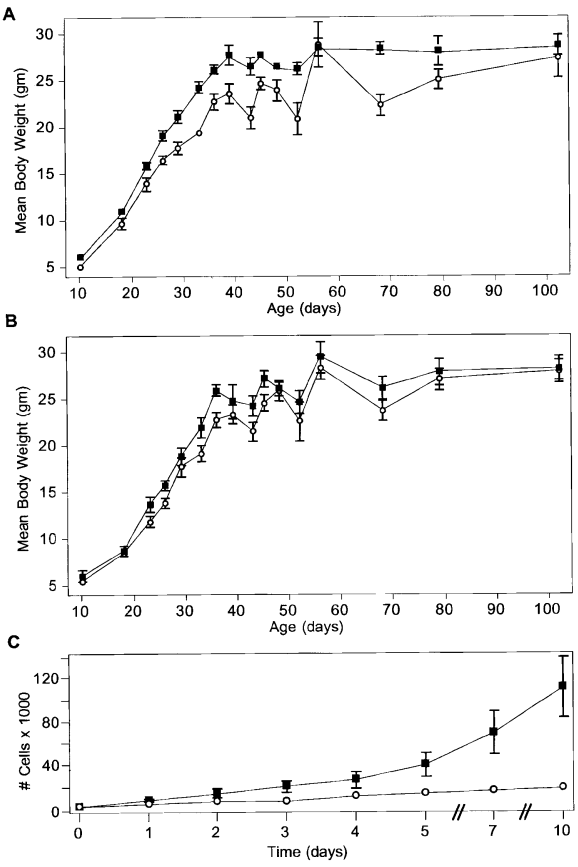

Figure 2. *Atm*-Disrupted Mice and Embryonic Fibroblasts Exhibit Growth Abnormalities

Mutant female (A) and male (B) mice weighed significantly less than their wild-type littermates from age 8 days to 3 months ($n = 241$, $p < 0.0001$). Embryonic fibroblasts from mutant mice were unable to grow under standard culture conditions (C). Error bars indicate the standard error of the mean, closed squares indicate wild-type animals or cells, and open circles indicate *Atm*-deficient animals or cells.

of wild-type mice and mice homozygous for the *Atm* disruption (Houldsworth and Lavin, 1980; Painter and Young, 1980). As expected, mutant tail fibroblasts displayed increased RDS ($p < 0.03$) after receiving 5 to 15 Gy of γ-irradiation when compared with wild-type tail fibroblasts (Figure 1D), similar to lymphoblastoid lines from AT patients (data not shown). This indicates that mice with the targeted mutation of *Atm* have abnormal Atm function.

Essential Role for *Atm* in Somatic Growth

Mice homozygous for the *Atm* disruption appeared to be smaller in size at birth. Daily inspection of the pups in these litters, until they could be unambiguously identified (postnatal day 8) and genotyped, confirmed that the majority of small mice identified at birth were homozygous mutants. We determined the growth of individual mice of all three genotypes from postnatal day 8 to 3 months of age. Overall, female (Figure 2A) and male (Figure 2B) mutant mice weighed significantly less ($p < 0.0001$) than wild-type littermates (total of 241 different mice). Body weights of heterozygous mice were similar to that of wild-type mice (data not shown). The difference was observed during nursing, after weaning, and during the period of rapid growth, suggesting that diet, competition for food, and physical problems with eating were not entirely responsible for the poor growth of the mutant mice. Instead, the abnormality appeared to be a direct effect of the disruption of *Atm* on cellular growth.

Poor Growth of Mutant Fibroblasts

Tail fibroblast lines from homozygous mutant mice used for RDS analysis grew slowly in culture using standard growth conditions and medium containing 10% fetal calf serum, while tail fibroblast lines from wild-type or heterozygous mice grew normally (data not shown). Human AT fibroblast lines grow slowly, undergo premature senescence, and have high requirements for growth factors (reviewed by Shiloh, 1995). We therefore made embryonic fibroblasts from a heterozygous cross and examined the growth properties of the cell lines prior to genotyping, so that our observations were blinded. All cell lines grew in 15% fetal calf serum over the first 2 or 3 days. However, after 3 days, two of the clones grew much more slowly than the other eight clones, and genotyping revealed that the two poorly growing clones were from homozygous mutant embryos. We measured the growth of these cells immediately after the first passage, and the mutant embryonic fibroblasts showed extremely poor growth (Figure 2C), while wild-type and heterozygous cells grew normally. In addition, three homozygous mutant lines from two other litters also grew poorly during expansion for genotyping (data not shown).

Neurologic Abnormalities in Mutant Mice

Mice homozygous for the disruption of *Atm* showed no gross ataxia. Therefore, rota-rod, open-field, and hindpaw footprint tests were used to characterize the motor responses of wild-type and mutant mice. These tests have been used successfully to identify motor impairments in knockout and transgenic mice with underlying cerebellar dysfunction (Chen et al., 1995; Conquet et al., 1994; Sango et al., 1995) or motor neuron degeneration (Gurney et al., 1994).

The rota-rod test was performed by placing each subject on a rotating drum and measuring the time the animal was able to maintain its balance on the rod. Mice were given two training trials to become accustomed to the apparatus. After 1 week, mice were given two trials with the rota-rod speed set at either 24 or 40 rpm. Wild-type mice were able to stay on the rota-rod significantly longer ($p < 0.01$) than mutant mice during the 24 and 40 rpm tests (Figure 3A). Heterozygotes performed similarly to wild-type mice (data not shown). Impaired rota-rod performance in mutant mice was not the result of poor strength, since all mice were able to remain suspended upside down from a wire lid for similar lengths of time (data not shown). There were no rota-rod performance differences between 2- and 4-month-old mutants (data not shown).

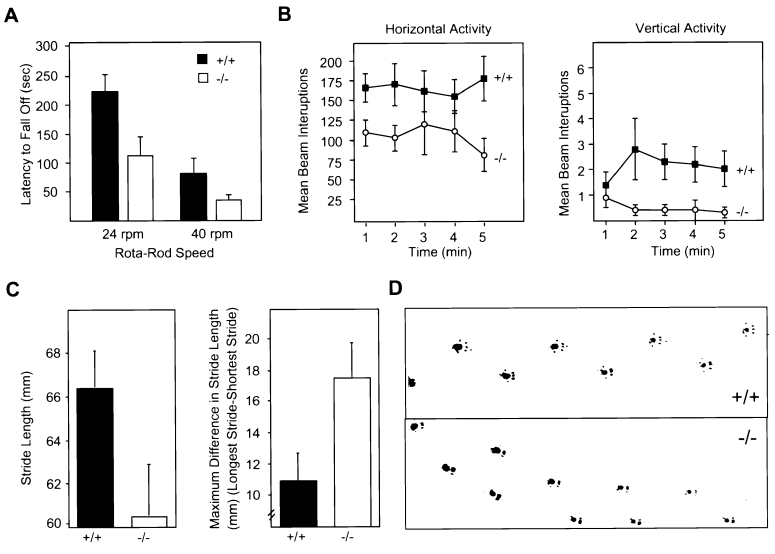

Figure 3. *Atm*-Disrupted Mice Demonstrate Behavioral Abnormalities Consistent with Cerebellar Dysfunction

Rota-rod testing (A) demonstrated that wild-type mice had significantly longer latencies to fall off the rota-rod than mutant mice ($F[1,24] = 7.858$, $p = 0.0099$). Open-field testing (B) demonstrated that wild-type mice were significantly more active compared with mutant mice as measured by horizontal activity ($F[1,24] = 5.89$, $p = 0.0231$), and they reared more often as measured by vertical activity ($F[1,24] = 4.847$, $p = 0.0376$). In (C), walking patterns were tested using the hind-paw footprint test. The average stride length was longer for wild-type mice than for the mutant mice ($t[24] = 1.892$, $p = 0.0353$, one-tailed test). Wild-type mice had more consistent stride lengths, as revealed in a significantly shorter maximum difference in stride length value compared with that seen with mutant mice ($t[24] = 2.166$, $p = 0.0405$). In (D), representative footprint patterns from a wild-type and a mutant mouse are shown. Top, wild-type mouse (+/+); bottom, *Atm*-disrupted mouse (−/−).

Spontaneous locomotor activity was measured using a standard open-field test. Wild-type and mutant mice were placed in the center of the open field, and their movement around the arena (horizontal activity) together with their rearing (vertical activity) behavior was measured for 5 min. Horizontal activity of the mutant mice was significantly less ($p < 0.05$) than that of wild-type controls (Figure 3B). Similarly, mutant mice reared less often ($p < 0.05$) than the wild-type mice.

Hind-paw footprint analysis was used to determine whether ambulation differed in mutant mice. The hind paws were first dipped in ink, and then the subject was placed at an open end of a tunnel. The mouse was allowed to walk to the other end of the tunnel, where it was retrieved and placed into its home cage. To characterize the walking pattern of each mouse, we measured the average distance between each stride (stride length). Mutant mice had significantly shorter ($p < 0.05$) stride lengths compared with the wild-type controls (Figure 3C), which in part could be due to their smaller size. However, the maximum difference in stride lengths (longest stride to shortest stride) was significantly greater ($p < 0.05$) in mutant mice (Figure 3C), which should be independent of size. This latter finding indicates that the stepping pattern in mutant mice was less consistent than in wild-type mice, indicative of ataxia (Figure 3D).

Histological analysis of brains from mutant mice at 1, 2, and 3 months of age showed normal architecture and no evidence of neuronal degeneration in brain, spinal cord, dorsal root ganglia, peripheral ganglia, and peripheral nerves by hematoxylin and eosin staining (data not shown). Examination of the cerebella of 2-month-old wild-type and mutant littermates stained with thionin, Bodian's silver stain, and Bielschowsky's silver stain showed normal Purkinje cell bodies, normal thickness of the granular cell and molecular layers, normal dendritic arborization, and no evidence of neuronal degeneration (data not shown). These results indicate that mice homozygous for the disruption of *Atm* were neurologically abnormal by several tests of motor function, but had no histological evidence of brain abnormalities, including normal cerebellar architecture, at 2 months of age.

Atm Is Essential for Germ Cell Development and Fertility

To determine the fertility of mice homozygous for the *Atm* disruption, we mated mutants with wild-type and heterozygous mice. Mutant males ($n = 5$) were capable of mating with control females in estrous, as demonstrated by the presence of a vaginal copulation plug. However, these matings never resulted in pregnancy ($n = 15$). These experiments demonstrated that male mutant mice had normal development of secondary sexual characteristics, and were capable of the mechanics of mating, but were infertile. Females homozygous for the *Atm* disruption ($n = 8$) were mated with wild-type and heterozygous males and checked daily for copulation plugs. Mutant females never had copulation plugs after 1 month, while all wild-type and heterozygous females in the same cages were plugged and became pregnant. In addition, 20 mutant females were checked on three separate occasions for estrous, indicative of normal ovulatory cycling, and none was in estrous at any time of observation, providing an explanation for the failure of males to mate with mutant females.

Mutant mice had grossly normal reproductive organs, except that the gonads of both sexes were extremely small. Histological examination of adult gonads from mutant mice of both sexes showed complete absence of mature gametes (Figure 4). Ovaries of wild-type females (Figures 4A and 4C) contained several primordial follicles, oocytes, and developing follicles, as well as stromal and interstitial cells between the follicles. In contrast, ovaries from mutant females were devoid of primordial and maturing follicles and oocytes (Figure 4B). The stroma contained numerous interstitial cells with clear vacuolated cytoplasm (Figure 4D). In addition, the uterine lining of mutant mice showed no evidence of proliferation or degeneration, indicative of a lack of estrous cycling.

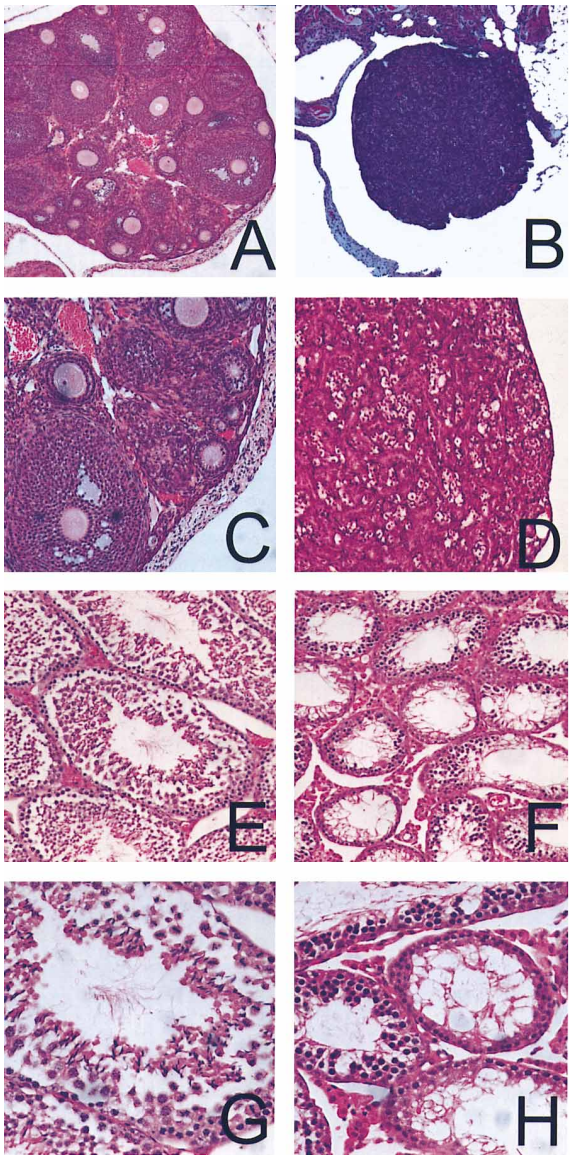

Figure 4. *Atm*-Disrupted Mice Are Infertile Secondary to a Complete Lack of Mature Gametes

Hematoxylin- and eosin-stained sections of ovaries from 2-month-old wild-type mice (A and C) and *Atm*-disrupted littermates (B and D). Sections of testes from 2-month-old wild-type mice (E and G) and *Atm*-disrupted mice (F and H). (A) and (B) are at 5× magnification, (C)–(F) are at 20× magnification, and (G) and (H) are at 40× magnification.

The normal architecture of 2-month-old wild-type testes (Figure 4E) demonstrates Leydig and supporting cells between the seminiferous tubules. The seminiferous tubules consist of a basement membrane, an outer layer of Sertoli cells and spermatogonia, several layers of maturing spermatocytes, spermatids, and mature sperm (Figure 4G). In contrast, testes from 2-month-old mutant littermates had complete disruption of spermatogenesis (Figure 4F). Leydig and supporting cells were normal in appearance and number in younger animals, but were increased in older mutants (data not shown). Although seminiferous tubules were present in mutant animals, they had reduced numbers of cells, evidence of cellular degeneration, and many were barren of all cell types except Sertoli cells (Figure 4H). Mutant seminiferous tubules were devoid of spermatids and spermatozoa. The epididymis was normal in structure, except that it was also devoid of spermatozoa (data not shown).

Immunologic Abnormalities in Mutant Mice

Lymphoid tissues from homozygous mutant mice were generally smaller in size when compared with the same tissues from littermate controls. However, histological analysis of thymus, spleen, lymph nodes, and bone marrow of wild-type, heterozygous, and mutant mice at 2, 4, and 8 weeks of age revealed no major difference in their architecture.

To investigate potential immunologic abnormalities, we performed flow cytometry analysis of thymocytes, splenocytes, lymph nodes, and peripheral blood from two wild-type, one heterozygote, and three mutant littermates at 2 months of age. Fewer cells were isolated from the tissues of mutant animals in comparison with controls, consistent with the smaller size of the mutant organs (data not shown). Cells from heterozygous and wild-type mice showed similar patterns of cell surface marker expression and were grouped as controls. Tissues were analyzed for expression of a variety of cell surface markers (Figure 5; Table 1). Thymocytes from mutant mice displayed a reduction in mature CD4 or CD8 single-positive T lymphocytes and an increase of immature double-positive thymocytes relative to control mice. Simultaneous analysis of CD3 in these cell populations confirmed that there was a 59% reduction of CD3/CD4 double-positive mature T lymphocytes in lymphoid tissues from the mutant mice as compared to control mice. Similarly, there was a 67% reduction in CD3/CD8 double-positive mature lymphocytes from cells of mutant as compared to cells from control mice. When thymocytes were analyzed simultaneously with CD5, CD4, and CD8, a similar reduction in mature T lymphocytes was observed in cells from mutant mice when compared with cells from control mice (data not shown). CD69 was used as a marker to identify activated T cells in lymph nodes and peripheral blood. Although the absolute numbers of CD3/CD69 and CD8/CD69 double-positive cells were reduced in mutant mice, double-positive cells were observed (data not shown), indicating that the few mature T lymphocytes present were capable of activation. Similar differences in mature T lymphocyte populations were obtained in cells from spleen, lymph nodes, and peripheral blood from control and mutant mice (Table 1). Finally, splenocytes and peripheral blood cells were analyzed by flow cytometry with CD45 (B220), a marker of B lymphocytes, and GR1 (myeloid differentiation antigen), a marker of granulocytes and myeloid cells but absent in erythroid and lymphoid cells. No differences were found (data not shown).

Development of Malignant Thymic Lymphomas in Mutant Mice

Between 2 and 4 months of age, mutant mice developed thymic lymphoblastic lymphomas. These tumors grew rapidly, causing death from compression of the heart and lungs or metastasis (or both). No mutant mouse has

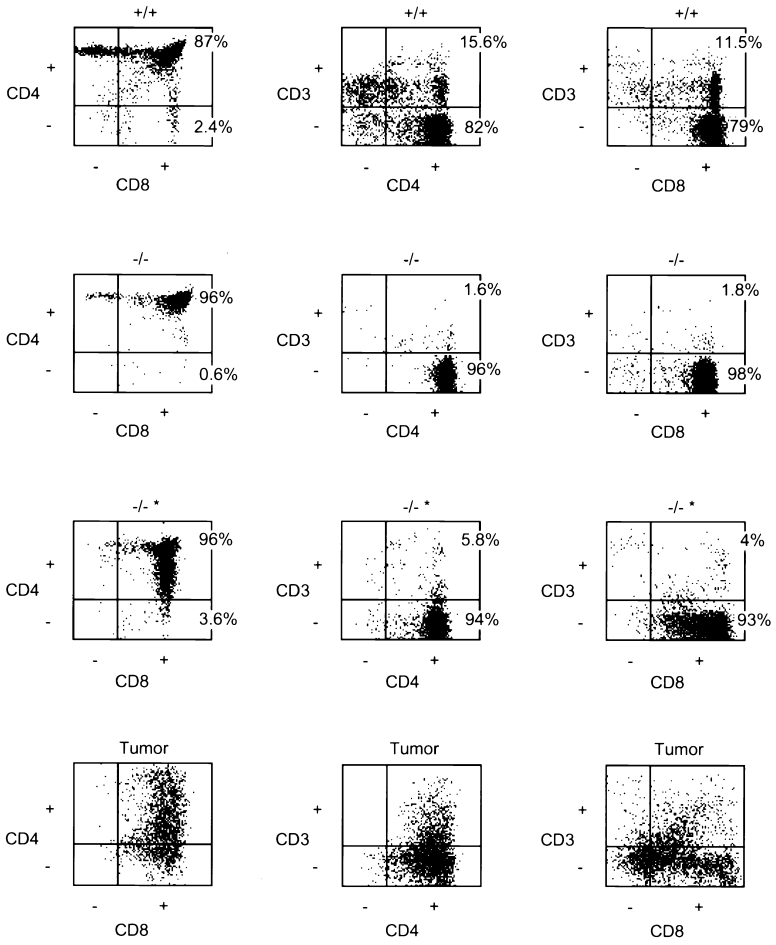

Figure 5. *Atm*-Disrupted Mice Have a Decrease in Mature T Cells and Develop Thymic Lymphomas

Thymocyte expression of CD3, CD4, and CD8 cell surface antigens was examined by three-color flow cytometry. Thymocytes from wild-type (+/+) and mutant mice (−/−), as well as thymocytes from a mouse with a microscopic focus of tumor (asterisk), and cells from a gross tumor are shown. Plus indicates positive and minus indicates negative for the cell surface antigens indicated to the left or below the graphs. Double-positive cell populations are represented in the upper-right quadrants and single-positive cells in the lower-right and upper-left quadrants. The value represents the percentage of cells in that quadrant.

survived beyond 4.5 months of age without a thymic lymphoma, and the youngest animal with a detectable tumor was 9 weeks old. In addition, all mutant mice that died spontaneously had massive lymphomas. We have observed and analyzed thymic tumors in more than ten mice. Histologically, the primary tumors consisted of monomorphic lymphoblastic cells (Figure 6A), with numerous mitotic figures (Figure 6B). Tumors were widely metastatic, resulting in the effacement of all tissues examined. One tumor invaded the subperiosteal space, as well as the bone marrow (Figure 6C), demonstrating its highly aggressive nature.

A cell line was readily established from one of these tumors. The line was IL-2 dependent and had a doubling time of 18–20 hr. Flow cytometry analysis of this tumor line revealed that it was $CD3^-$, $CD4^+$, and $CD8^+$ (Figure 5), as well as $CD5^-$ (data not shown). When performing flow cytometry analysis on a healthy-appearing 2-month-old mutant mouse, we observed a population of cells similar in appearance to the tumor cells (Figure 5), which likely represent cells from an early tumor. These cells were not found in any other organ (data not shown), confirming the thymic origin of the primary tumor. Thus, the tumor consists of immature T cells and is completely consistent with the histological diagnosis of thymic lymphoblastic lymphoma.

We determined the karyotypic abnormalities of this tumor cell line early in culture (passage 2) by spectral karyotyping (SKY), a method that allows simultaneous, unambiguous identification of each chromosome using

Table 1. Flow Cytometry Analysis of Wild-Type and *Atm*-Deficient Thymocytes, Splenocytes, Lymph Node Cells, and Peripheral Blood

Sample	$CD4^+/CD8^+$	$CD3^+/CD4^+$	$CD3^+/CD8^+$	$CD3^+/CD69^+$
Control thymus	91.48 ± 2.17	9.12 ± 3.22	9.42 ± 1.05	13.95 ± 2.66
Mutant thymus	96.89 ± 0.57	3.77 ± 1.28	3.14 ± 1.08	5.22 ± 1.06
Control spleen	10.22 ± 1.15	16.76 ± 1.63	30.24 ± 1.96	5.39 ± 0.87
Mutant spleen	6.59 ± 0.56	13.15 ± 1.05	21.20 ± 1.66	5.21 ± 1.46
Control lymph node	5.01 ± 0.20	18.63 ± 2.11	20.12 ± 3.88	8.68 ± 1.58
Mutant lymph node	5.57 ± 0.16	12.14 ± 1.97	11.11 ± 1.27	6.39 ± 0.77
Control blood	0.57	16.75	13.01	16.52
Mutant blood	0.52	2.70	1.04	3.18

Values represent percent double-positive cells ± standard error of the mean. n = 3 for all samples, except blood where n = 2.

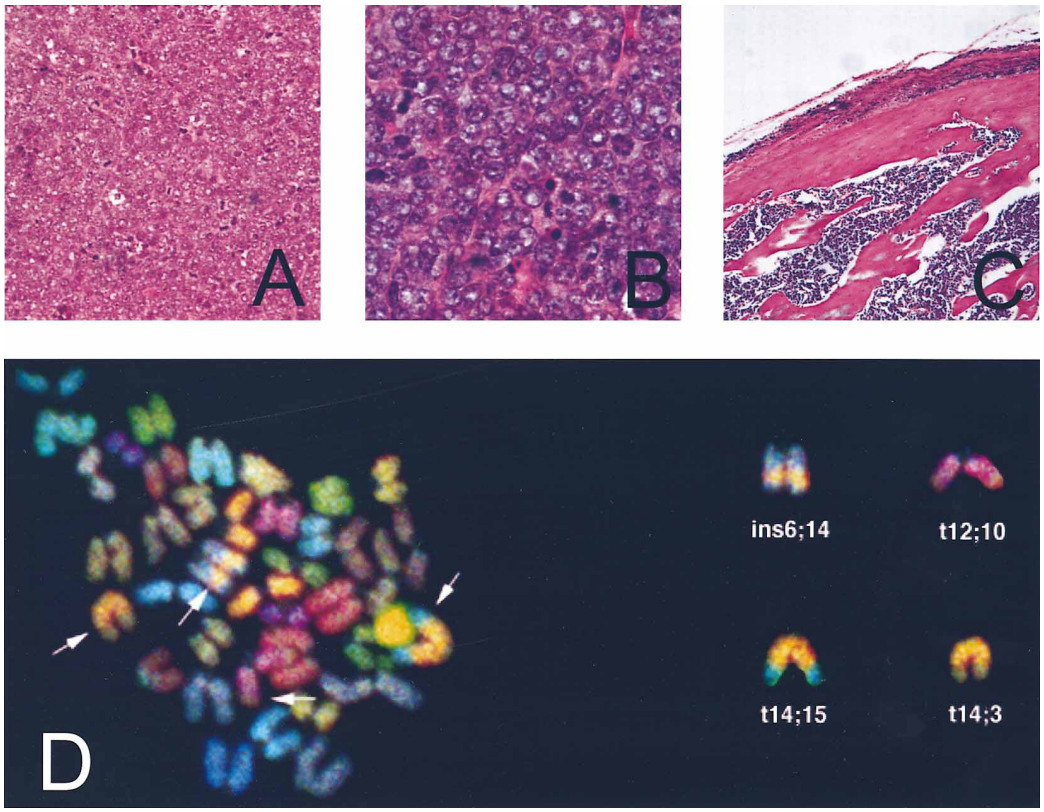

Figure 6. *Atm*-Disrupted Mice Develop Thymic Lymphoblastic Lymphomas

Hematoxylin- and eosin-stained section of a representative tumor are shown. Primary tumors consisted of monomorphic lymphoblastic cells (A), with numerous mitotic figures (B). The tumor has invaded the subperiosteal space, as well as the bone marrow (C). (D) demonstrates chromosomal aberrations found in tumor cells using SKY. One metaphase spread is shown on the left, and specific chromosomes with aberrant arrangements are shown on the right.

individual chromosome-painting probes (Schröck et al., 1996b). Using SKY and mouse chromosomal–painting probes, all mouse chromosomes can be analyzed and identified simultaneously in metaphase spreads and each displayed using a different color (M. L. and T. R., unpublished data). No aberrations were detected in control hybridizations to metaphase chromosomes from normal mice (data not shown). The analysis of metaphase spreads from primary cultures of the thymoma revealed multiple, recurrent rearrangements (Figure 6D). In all ten metaphases analyzed, the following aberrations were detected: translocations t(12;10), t(14;13), and t(14;15) as well as an insertion, ins(6;14). Since the analysis was performed on early passage cells, it most likely reflects karyotypic abnormalities intrinsic to the tumor.

Extreme Radiation Sensitivity of *Atm* Mutant Mice

We determined the sensitivity of mice homozygous for the *Atm* disruption to ionizing radiation. Primary embryonic fibroblasts from mutant mice grow poorly, so the analysis of radiation sensitivity using survival assays might be prone to misleading artifact. Therefore, 10-week-old wild-type, heterozygous, and homozygous mutant littermates were irradiated with two different doses of γ-irradiation, and the mice were monitored for morbidity and mortality. At a dose of 8 Gy (Figure 7A), about two thirds of wild-type and heterozygous mice died. Most of these animals died suddenly, beginning 6 days postirradiation, and some died as late as 18 days postirradiation. The time course of death was consistent with bone marrow depletion of white blood cells and concomitant infection. In contrast, all mutant mice irradiated at 8 Gy died 3–5 days postirradiation (Figure 7A). Prior to death, mutant mice developed diarrhea and showed evidence of peritoneal inflammation.

At a dose of 4 Gy (Figure 7B), all heterozygous and wild-type mice survived the 4 week duration of the experiment without any morbidity. In a separate experiment, 23 heterozygous and 15 wild-type mice were irradiated with 4 Gy and are without morbidity after 2 months (data not shown). In contrast, two thirds of the mutant mice irradiated at 4 Gy died between 5 and 7 days, with similar abdominal symptoms (Figure 7B). The remaining third were without morbidity after 4 weeks.

To determine the cause of death, we irradiated wild-type and mutant mice with 8 Gy, and examined various tissues histologically at 2, 3, and 4 days postirradiation. Most tissues were histologically normal in appearance. For example, brain, skin, lung, heart, skeletal muscle, pancreas, bone, and cartilage were unaffected by this dose of radiation in control and homozygous mutant mice (data not shown). The thymus, spleen, lymph

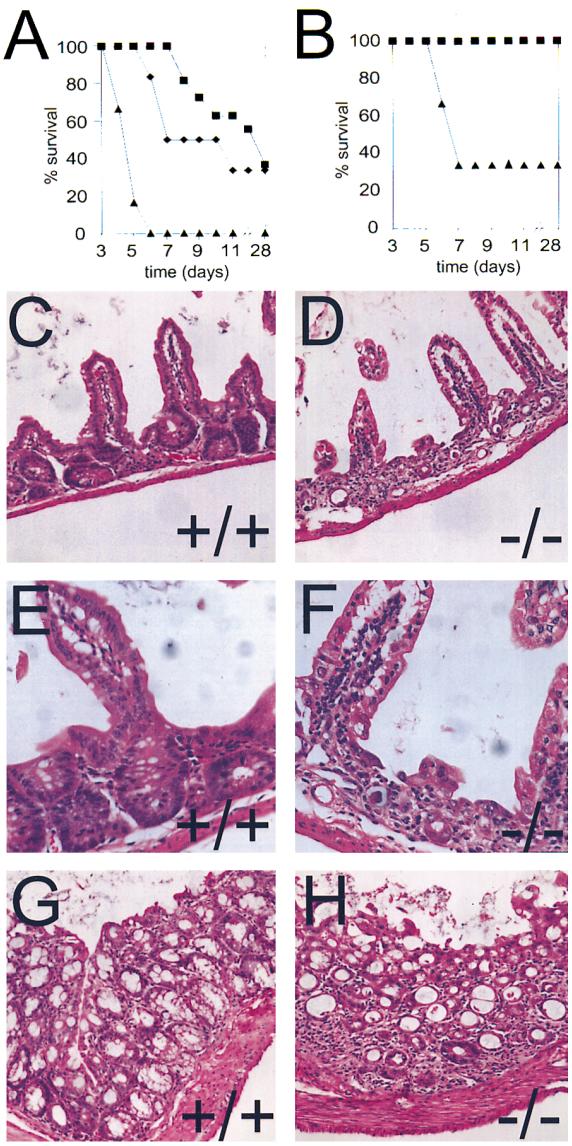

Figure 7. *Atm*-Disrupted Mice Are Acutely Sensitive to Ionizing Radiation

Shown are survival curves of mice after irradiation with either 8 Gy (A) or 4 Gy (B). Wild-type mice are indicated by closed diamonds, heterozygous mice by closed squares, and *Atm*-disrupted mice by closed triangles. Shown below are hematoxylin- and eosin-stained sections of the small intestine (C–F) and large intestine (G and H) from a wild-type (C, E, and G) and mutant (D, F, and H) mouse 4 days after a dose of 8 Gy was given. (C) and (D) are at 20× magnification, and (E)–(H) are at 40× magnification.

nodes, and bone marrow, tissues known to be sensitive to γ-irradiation, were depleted of cells in both control and mutant mice, although the mutant mouse lymphoid tissues were slightly more cellular than control mouse tissues (data not shown). Thus, the rapid death of mutant mice was unlikely to result from more severe effects on immune function in the mutant mice.

The death of the mutant mice resulted from acute radiation toxicity to the gastrointestinal tract. In the stomach, mutant and wild-type mice both had parietal cell degeneration, which was more severe in mutant mice at 2 days postirradiation (data not shown). In the intestines, wild-type mice 2 (data not shown) and 4 days (Figures 7C and 7E) postirradiation had minimal to mild epithelial crypt degeneration. In contrast, intestines from mutant mice displayed severe radiation toxicity. At 2 days postirradiation (data not shown), there were moderate degrees of epithelial crypt degeneration, as well as crypt abscesses consisting of degenerating crypt epithelial cells and polymorphonuclear cells. By 4 days postirradiation (Figures 7D and 7F), villi were blunted and shortened, and there were some areas where crypts were entirely obliterated. Dilated degenerative crypts were frequently observed (Figure 7F). There were occasional regions of erosion and ulceration. Changes 3 days postirradiation were intermediate (data not shown). The colon of wild-type mice irradiated at 8 Gy was unaffected at 2 days (data not shown) and minimally affected at 4 days (Figure 7G) postirradiation, as evidenced by occasional degenerating cells. Mutant mice at 2 days postirradiation with 8 Gy (data not shown) showed evidence of mild epithelial degeneration, progressing to a moderate loss of glandular epithelium by 4 days (Figure 7H). In addition, there was evidence of increased radiation sensitivity of the salivary glands in mutant mice. This finding was specific to the salivary gland, as no ductal degeneration was evident in the pancreas (data not shown).

Thus, *Atm*-deficient mice are exquisitely sensitive to ionizing radiation. Death was caused by the severe toxic effects of radiation on the gastrointestinal tracts. Surprisingly, there was selective acute toxicity of specific tissues of mutant mice to γ-irradiation, rather than global radiation toxicity.

Discussion

We have created mice with a disruption of *Atm*, which recapitulates the human disease and points to a critical role of *Atm* in the maintenance of mitotic, postmitotic, and meiotic cells. Mice homozygous for the *Atm* disruption have growth retardation, neurologic dysfunction, infertility, immunologic abnormalities, lymphoreticular malignancies, chromosomal instability, and extreme sensitivity to ionizing radiation. The only characteristic phenotype of AT not seen in these mice are oculocutaneous telangiectasias, as determined by gross observation and histological sectioning of the eyes (data not shown). These often appear later in the progression of the disease and may be a consequence of sun exposure (Boder, 1975).

We have noticed no abnormalities in heterozygous mice up to 8 months of age. They are of normal size and fertility and free of tumors and illness. They are no more sensitive to the acute effects of ionizing radiation than wild-type mice, and no morbidity has been noted up to 2 months postirradiation. We are currently following a cohort of irradiated heterozygotes and wild-type mice to determine whether irradiation causes an increased tumor frequency in heterozygotes.

The homozygous mutant mice have neurologic deficits as assessed by poor performance on three separate tests of motor function. That three disparate measures

of motor function are abnormal strongly suggests they have neurologic deficits, as found in persons with AT (Boder, 1975; Sedgewick and Boder, 1991; Shiloh, 1995). However, we observed no histological evidence of neuronal degeneration. Histological changes early in the course of AT have not been examined. The characteristic Purkinje cell body degeneration seen in end-stage brains from AT patients postmortem may be a late manifestation. Since mutant mice succumb to tumors, they may not live long enough to show gross signs of ataxia and histological signs of neuronal degeneration. We are attempting to prolong the lives of mutant mice by strategies to eliminate the thymic lymphomas.

Although unlikely, it is possible that the behavioral abnormalities in the mutant mice are not a consequence of neuronal abnormalities. For example, impairments resulting from illness in the mutants as tumors develop may lead to reduced performance on the rota-rod. However, all mice tested were alive and tumor free 4 weeks after the test was completed. In addition, one mutant mouse tested by open-field and footprint analysis had a tumor, yet performed as well or better than other mutant animals. In any case, the *Atm*-deficient mice exhibit consistent and clear evidence of neurologic dysfunction by several independent tests.

The mutant mice have reduced T cell receptor–bearing T cells. AT patients also have alterations in T cell receptor–bearing populations of mature lymphocytes (Carbonari et al., 1990). In addition, mutant mice uniformly develop aggressive malignant thymic lymphoblastic lymphomas, similar to the predisposition to lymphoreticular malignancies in patients with AT (Boder, 1975; Sedgewick and Boder, 1991) and thymic tumors in p53 null mice (Donehower et al., 1992; Jacks et al., 1994; Purdie et al., 1994; Tsukada et al., 1993). In humans, these malignancies are associated with chromosomal rearrangements near T cell receptor genes (Heppell et al., 1988; Metcalfe et al., 1991; Russo et al., 1988; Sherrington et al., 1994; Stern et al., 1989; Thick et al., 1992). The tumor cell line derived from the thymic lymphoma from one of the mutants contains chromosomal aberrations, as detected by SKY, and some rearrangements occur near T cell receptor genes. For example, the t(14;13) is close to the T cell receptor α/δ genes on mouse chromosome 14, the ins(6;14) is near the T cell receptor β and immunoglobulin κ genes on chromosome 6, and the t(12;10) is close to the immunoglobulin heavy chain gene. Of note, the high number of chromosomal aberrations in this primary thymic lymphoma suggests a high degree of genomic instability, as seen in normal and tumor tissue from AT patients (Kojis et al., 1991; Taylor et al., 1981).

It is reasonable to speculate that the thymocyte maturational defect and the thymic malignancies are mechanistically related, as a result of abnormalities in DSB repair characteristic of cells from AT patients (Meyn, 1995; Shiloh, 1995). In particular, Atm or ATM may participate in the repair of DSBs introduced in the T cell receptor gene rearrangements during normal maturation. Defects in this process would lead to the inability of immature thymocytes to synthesize active T cell receptors and mature fully. Abnormal repair of these DSBs would result in occasional translocations involving proto-oncogenes, leading to the development of thymic malignancies. Such a model is supported by the phenotype of *Atm*-deficient mice and AT patients.

Disruption of *Atm* results in complete infertility of both sexes due to the lack of mature gametes. A similar phenotype has been observed but poorly studied in many AT patients. Some patients develop secondary sexual characteristics. Females may ovulate, but most are anovulatory, and males have testicular atrophy and disrupted spermatogenesis (Boder, 1975; Sedgewick and Boder, 1991). The severity of the gametogenesis defects suggests that *Atm* acts in spermatogonia and primordial follicles. This is consistent with the expression pattern of *Atm* by in situ hybridization analysis. *Atm* is expressed in the follicles of the adult ovaries and the spermatogonia of the adult testes (S. Marquis and L. Chodosh, personal communication). Preliminary analysis has shown that the spermatocytes of mutant testes and the primordial follicles in mutant ovaries degenerate at the time of prophase of meiosis I in gametogenesis, temporally associated with the onset of meiotic recombination (unpublished data). The meiotic recombination defects observed in *MEC1* mutants in S. cerevisiae (Kato and Ogawa, 1994) and *mei41* mutants in D. melanogaster (Baker and Carpenter, 1972) would support a role for *Atm* in meiotic recombination. The coincident finding of thymocyte maturational defects and gonadal degeneration suggests a mechanistic connection between meiotic and immune recombinational pathways.

The increase in RDS in tail fibroblasts from mutant mice indicates that disruption of *Atm* function results in G1/S checkpoint abnormalities, similar to observations made in AT cell lines (Houldsworth and Lavin, 1980; Painter and Young, 1980). In AT cell lines, this defective radiation-induced checkpoint is associated with defective induction of p53 protein and *gadd45* (Artuso et al., 1995; Kastan et al., 1992). p53 may have a direct or indirect role in DNA repair processes, since p53-deficient cells and tumors show chromosomal rearrangements (Lane, 1992) and enhanced gene amplification (Livingstone et al., 1992; Yin et al., 1992). Some DSB repair defects seen in AT may be mediated by p53, either directly through binding to recombination proteins (Sturtzbecher et al., 1996) or secondary to checkpoint control (Dulic et al., 1994; Kuerbitz et al., 1992). In addition to RDS, mutant mice were severely affected by doses of radiation that had no effect on control mice. The gastrointestinal tract and salivary glands showed the greatest sensitivity. The remaining tissues were unaffected, demonstrating that selective tissues depend upon *Atm* function for acute postirradiation survival, while most tissues are not acutely sensitive to loss of *Atm* function. It has been proposed that *Atm* may act through p53 in lymphoid tissues (Clarke et al., 1993; Lowe et al., 1993) and gut (Clarke et al., 1994) to provide appropriate apoptotic responses to ionizing radiation. However, p53-deficient mice are not acutely sensitive to 4 Gy of irradiation (Kemp et al., 1994), whereas this dose caused rapid death due to gut toxicity in two thirds of *Atm*-disrupted mice. This suggests that some functions of *Atm* or *ATM* may be p53 independent.

Growth retardation was a prominent feature of mutant mice and is also consistently found in patients with AT

(Boder, 1975; Sedgewick and Boder, 1991). This observation suggests an intrinsic growth-promoting function of *Atm*. In support of this, mutant adult and embryonic fibroblast lines grew poorly in culture and had a flattened morphology, with increased amounts of cell death. These growth abnormalities may be the result of defects in DSB repair, cell cycle–regulatory defects, or both. Potential downstream effectors of *Atm* are the Rel/NF-κB/IκB family of transcription factors (reviewed by Verma et al., 1995), since a truncated fragment of IκB rescued the cellular phenotype of an AT cell line (Jung et al., 1995). c-*jun* may participate in the growth-promoting properties of *Atm*, since c-*jun*-deficient fibroblasts have a similar phenotype (Johnson et al., 1993). Of interest, c-*jun* appears to participate in checkpoint control and cell survival after exposure to ionizing radiation (Hallahan et al., 1995). In contrast to *Atm*-deficient fibroblasts, p53- or p21-deficient fibroblasts reach higher saturation densities in culture than wild-type cells (Brugarolas et al., 1995; Deng et al., 1995). The growth retardation of mice and poor growth of cells in culture can be used to determine whether factors such as IκB, p53, p21, c-*jun*, or others participate in *Atm*-mediated growth pathways.

How might the diverse functions of *Atm* and *ATM* shed light on the devastating neurological degeneration so characteristic of AT? As previously suggested (Heintz, 1993), postmitotic neurons, when damaged, activate signal transduction cascades that result in cell death. The damage-response pathways may be regulated by cell cycle checkpoint genes that monitor DNA damage and cause cell cycle arrest of mitotic cells. Although there is no evidence that neurons have increased levels of DSBs, postmitotic neurons in brains of AT patients may accumulate DNA damage at a fixed rate from the failure of repair mechanisms. Over time, if sufficient damage is unrepaired, cell death pathways may be activated.

Given the complicated phenotypes of persons with AT and the *Atm*-deficient mice, it is not currently possible to devise a unifying model to encompass the diverse and pleiotropic actions of *Atm* and *ATM*. These genes, and their lower eukaryotic homologs, are intimately involved in the appropriate functioning of a variety of postmitotic, mitotic, and meiotic cells, as well as fundamental processes such as DSB repair, meiotic recombination, and cell cycle control. Our analysis of this mouse with the disruption of *Atm* function, and the comparison of the phenotype with that of persons with AT, suggests a framework for understanding relationships among these diverse processes. This mouse provides an excellent model for understanding the role of *Atm* in normal cellular function as well as pathophysiology and for testing potential therapeutic agents to treat the progressive, debilitating manifestations of AT.

Experimental Procedures

Gene Targeting and Generation of *Atm*-Disrupted Mice

A 236 bp PCR fragment corresponding to nucleotides 5381–5617 of human *ATM* (Savitsky et al., 1995b), where 3 of 11 initial mutations were described previously (Savitsky et al., 1995a), was tested on mouse genomic Southern blots, and conditions were established that yielded a single hybridizing band (data not shown). This fragment was used to screen a mouse genomic library made from 129/Sv mice (Stratagene). Two overlapping clones were isolated and characterized. Two exons were detected in these overlapping clones (Figure 1A), and one of 178 bp (corresponding to nucleotides 5705–5881) was used.

A targeting construct (Figure 1A) was made by inserting a PGK*neo* gene into the 178 bp exon at an FspI site, in an opposite orientation relative to *Atm* transcription using a pPNT backbone and 8.5 kb of homology (Tybulewicz et al., 1991). The vector was linearized and transfected into TC1 embryonic cells as described previously (Deng et al., 1996). We screened 120 G418- and FIAU-resistant clones by Southern blot analysis using a flanking probe (Figure 1A); five positive clones were detected (Figure 1B). Extensive restriction analysis using flanking and internal probes showed that all were correctly targeted (data not shown).

Targeted clones were injected into C57BL/6J blastocysts by standard methods (Hogan et al., 1994). One clone gave high level chimeras, which transmitted the disrupted *Atm* allele to offspring at high frequency, allowing this allele ($Atm^{ins5790neo}$) to be established in a mixed (129/SvEv × NIH Black Swiss) or completely inbred (129/SvEv) background. As described previously (Deng et al., 1994), NIH Black Swiss mice were used to determine germline transmission. Genotyping was performed by Southern blot analysis with either the flanking probe described above or a probe derived from genomic DNA surrounding the targeted exon. All mouse experiments were carried out with the NCHGR Animal Care and Use Committee approval and in compliance with ALAC regulations.

Primary Cell Culture

Fibroblasts were isolated from tail biopsies. The biopsy specimen was minced, digested in collagenase and trypsin, and plated in Dulbecco's modified Eagle's medium (DMEM), 10% heat-inactivated fetal calf serum, 100 mM L-glutamine, and 5× antibiotics (penicillin and streptomycin). Cells were passaged 1:2 and used for RDS experiments.

Embryonic fibroblasts were isolated by standard procedures (Hogan et al., 1994). Heterozygous females were mated to heterozygous males, and embryos were isolated at day 12.5 after mating. Cultures of individual embryos were grown in DMEM, 15% heat-inactivated fetal calf serum, 100 mM L-glutamine, and 5× antibiotics on individual plates until they reached confluence (4–5 days). Cells were either frozen at this point (passage 1) or plated for DNA isolation, growth experiments, or both.

Each cell line was passaged, and equal numbers (4×10^4) were plated into individual 6-well wells (14 for each line). Medium was changed daily. Duplicate wells of each line were counted using a hemocytometer, and the average cell number was plotted versus days in culture.

A sample of the malignant thymic lymphoma was disrupted and plated at various densities in RPMI, 10% heat-inactivated fetal calf serum, 100 mM L-glutamine, 5× antibiotics, and IL-2 (100 U/ml). Cells were split 1:2 and 1:4 until established.

Animal Growth Measurements

Heterozygous crosses were used to generate mice for experiments. At postnatal day 8, pups were marked for identification by ear tagging. Weights were initiated prior to genotyping by Southern blot analysis, and mice were weighed weekly until 3 months of age. After weaning, animals were housed with littermates of the same sex, and food was provided ad libitum.

Behavioral Methods

Mice were tested during the light phase of their light–dark cycle between 1030 and 1600. The rota-rod (rod diameter, 30 mm) was a UGO Basile Accelerating rota-rod for mice (model 7650, Stoelting). Wild-type (seven males and seven females) and mutant mice (eight males and four females) were given two training trials (intertrial interval, 2 hr) with the rota-rod adjusted to accelerate from 6 rpm to 40 rpm over a 5 min period. Latency to fall off was measured. After 1 week, mice were tested using the rota-rod adjusted to maintain a constant speed for the entire 5 min test period. Each mouse was first tested with the rota-rod set at 24 rpm followed 1 hr later with the speed increased to 40 rpm. Open-field activity was measured using a clear plexiglas (40 cm × 30 cm × 30 cm) chamber. Activity

was measured using a Digiscan optical animal activity monitor (model RXYZ, Omnitech Electronics), which records the number of times a beam of light is interrupted. Four male and seven female wild-type mice were tested together with seven male and eight female mutant mice. A native wild-type or mutant mouse was placed in the center of the arena and its activity was monitored for 5 min. Each minute, the horizontal (movement and locomotion around the arena) and vertical (rearing) activity was recorded. Immediately after testing in the open field, the back paws of each mouse were dipped into black ink, and it was placed at the entry of a dark tunnel (9.2 cm $\times$ 6.3 cm $\times$ 35.5 cm). The footprints were recorded on a clean sheet of white paper placed in the floor of the tunnel. Stride lengths were determined by measuring the distance between each step on the same side of the body (e.g., the distance between one right footprint and the next right footprint). Average stride length was calculated. The distance of the shortest stride was subtracted from the distance of the longest stride to determine the maximum difference in stride length for each subject.

Histopathological Analysis

Tissues were collected and placed in 20 vol of 10% buffered formalin. Fixed tissues were embedded in paraffin blocks, sectioned, and stained using standard methods (Luna, 1992) by American Histology Labs (Gaithersburg, MD). Sections were examined and photographed under light microscopy.

Flow Cytometry Analysis

Thymus, spleen, lymph nodes, and peripheral blood were harvested from two wild-type, one heterozygote, and three mutant 2-month-old mice by standard methods (Harlow and Lane, 1988). Thymocytes, splenoctyes, and lymph node cells were mixed with various antibodies conjugated to either fluorescein isothiocyanate (FITC), R-phycoerythrin (PE), or CyChrome for use in three-color analysis as follows: anti–CD3 CyChrome, anti–CD4 PE, anti–CD8 FITC; anti–CD3 CyChrome, anti–CD69 PE, anti–CD8 FITC; anti–CD5 CyChrome, anti–CD4 PE, anti–CD8 FITC; and anti–CD45R CyChrome, anti–GR-1 FITC (Pharmingen). Peripheral blood was mixed with either anti–CD3 CyChrome, anti–CD4 PE, anti–CD8 FITC, or anti–CD45R CyChrome and anti–GR-1 FITC. Appropriate isotypic controls were used to set flow cytometer compensation.

SKY

Metaphase chromosomes were prepared using standard procedures (Schröck et al., 1996a). The mouse chromosome-specific painting probes were generated from flow-sorted mouse chromosomes (Rabbitts et al., 1995). DNA labeling was performed as described by Schröck et al. (1996b). In situ hybridization was performed by combining the labeled DNA pools with an excess of a Cot-1 fraction of mouse DNA (Bethesda Research Labs). Hybridization conditions, posthybridization washes, and immunological detection steps were performed as described previously (Schröck et al., 1996b).

Multicolor hybridization was visualized using SKY (Schröck et al., 1996b). In brief, using a combination of Fourier spectroscopy, CCD imaging, and optical microscopy, the spectrum of the emitted light was measured at each pixel of the image to assign a specific spectrum to each chromosome. The measurement of specific emission spectra then allows the simultaneous display of all mouse chromosomes, each with a different color.

Irradiation Experiments

Animals and cells were irradiated in a Gammacel 3000 Elan model II irradiator (Nordion International, Inc.), with a ^{137}Cs source at a rate of 21.6 rads/s. Littermates were irradiated in single doses of either 4 Gy or 8 Gy (1 Gy = 100 rads), and survival was determined. At each radiation dose, 6 wild-type, 12 heterozygous, and 6 mutant mice were irradiated and compared with a cohort of nonirradiated mice. In a separate experiment, 3 wild-type and 3 homozygous mutant mice were irradiated at 8 Gy, and 1 of each genotype sacrificed after 2, 3, and 4 days. Tissues were isolated, fixed, and analyzed as described.

To determine the fidelity of the G1 checkpoint in cells with disrupted *Atm* function, tail fibroblasts (passage 1) were analyzed for RDS. Three tail fibroblast lines of each of the three *Atm* genotypes were plated in 96-well tissue culture plates at 8000 cells per well. The next day, medium was replaced. After 4 hr, cells were irradiated at 0, 5, and 10 Gy, 10 μCi of [^{3}H]thymidine was added to each well, incubated for 4 hr, and frozen, and [^{3}H]thymidine incorporation was determined. The [^{3}H]thymidine incorporation in unirradiated cells was set at 100%, and percent incorporation was calculated.

Statistical Analysis

Analyses of variance (ANOVA) were used to analyze data from rotarod and open-field activity tests. Post hoc comparisons were made using either Newman–Keuls or simple effects tests. Stride length data were analyzed using a one-tailed t test, and maximum difference in stride using a two-tailed t test. A three-way ANOVA (genotype $\times$ gender $\times$ day) was used to analyze the body weight data. A two-way ANOVA with repeated measures (genotype $\times$ dose) was used to analyze the RDS data.

Acknowledgments

The authors are grateful to Lisa Garrett, Theresa Hernandez, David Bernard, and Cheral Canna for crucial technical support in making the disrupted mice; Mona Schroeder, Lisa Pike-Buchanan, and Denise Larson for excellent technical assistance; Stacie Anderson and Pam Schwartzberg for advice and assistance with flow cytometry; M. A. Ferguson-Smith for providing mouse chromosome–specific painting probes; Allen Coleman for help with mouse chromosome identification; and Bart Williams for comments on the manuscript. C. B. is a Clinical Endocrine Fellow supported by the National Institute of Diabetes, Digestive, and Kidney Diseases. In particular, the advice and interest of Brad Margus and The AT Children's Project were invaluable.

Received June 7, 1996; revised June 21, 1996.

References

Artuso, M., Esteve, A., Bresil, H., Vuillaume, M., and Hall, J. (1995). The role of the ataxia telangiectasia gene in the p53, WAF1/CIP1(p21)- and GADD45-mediated response to DNA damage produced by ionizing radiation. Oncogene *11*, 1427–1435.

Baker, B.S., and Carpenter, A.T.C. (1972). Genetic analysis of sex chromosomal meiotic mutants in *Drosophila melanogaster*. Genetics *90*, 255–286.

Blocher, D., Sigut, D., and Hannan, M.A. (1991). Fibroblasts from ataxia telangiectasia (AT) and AT heterozygotes show an enhanced level of residual DNA double-strand breaks after low dose-rate γ-irradiation as assayed by pulsed field gel electrophoresis. Int. J. Radiat. Biol. *60*, 791–802.

Boder, E. (1975). Ataxia-telangiectasia: some historic, clinical and pathologic observations. Birth Defects *11*, 255–270.

Brugarolas, J., Chandrasekaran, C., Gordon, J.I., Beach, D., Jacks, T., and Hannon, G.J. (1995). Radiation-induced cell cycle arrest compromised by p21 deficiency. Nature *377*, 552–557.

Byrd, P.J., McConville, C.M., Cooper, P., Parkhill, J., Stankovic, T., McGuire, G.M., Thick, J.A., and Taylor, A.M.R. (1996). Mutations revealed by sequencing the 5′ half of the gene for ataxia-telangiectasia. Hum. Mol. Genet. *5*, 145–149.

Carbonari, M., Cherchi, M., Paganelli, R., Giannini, G., Galli, E., Gaetano, C., Papetti, C., and Fiorilli, M. (1990). Relative increase of T cells expressing the γ/δ rather than the α/β receptor in ataxia-telangiectasia. N. Engl. J. Med. *322*, 73–76.

Chen, C., Kano, M., Abeliovich, A., Chen, L., Bao, S., Kim, J.J., Hashimoto, K., Thompson, R.F., and Tonegawa, S. (1995). Impaired motor coordination correlates with persistent multiple climbing fiber innervation in PKCγ mutant mice. Cell *83*, 1233–1242.

Clarke, A.R., Purdie, C.A., Harrison, D.J., Morris, R.G., Bird, C.C., Hooper, M.L., and Wyllie, A.H. (1993). Thymocyte apoptosis induced by p53-dependent pathways and independent pathways. Nature *362*, 849–852.

Clarke, A.R., Gledhill, S., Hooper, M.L., Bird, C.C., and Wyllie, A.H.

(1994). p53 dependence of early apoptotic and proliferative responses within the mouse intestinal epithelium following γ-irradiation. Oncogene *9*, 1767–1773.

Conquet, F., Bashir, Z.I., Davies, C.H., Daniel, H., Ferraguti, F., Bordi, F., Franz-Bacon, K., Reggiani, A., Matarese, V., Conde, F., Collingridge, G.L., and Crepel, F. (1994). Motor deficiency and impairment of synaptic plasticity in mice lacking mGluR1. Nature *372*, 237–243.

Coquerelle, T.M., Weibezahn, K.F., and Lucke-Huhle, C. (1987). Rejoining of double strand breaks in normal human and ataxia-telangiectasia fibroblasts after exposure to ^{60}Co γ-rays, ^{241}Am α-particles or bleomycin. Int. J. Radiat. Biol. Relat. Stud. Phys. Chem. Med. *51*, 209–218.

Cox, R., Debenham, P.G., Masson, W.K., and Webb, M.B. (1986). Ataxia-telangiectasia: a human mutation giving high-frequency misrepair of DNA double-stranded scissions. Mol. Biol. Med. *3*, 229–244.

Deng, C., Wynshaw-Boris, A., Shen, M.M., Daugherty, C., Ornitz, D., and Leder, P. (1994). Murine FGFR1 is required for early postimplantation growth and axial organization. Genes Dev. *8*, 3045–3057.

Deng, C., Zhang, P., Harper, J.W., Elledge, S.J., and Leder, P. (1995). Mice lacking p21$^{CIP1/WAF1}$ undergo normal development, but are defective in G1 checkpoint control. Cell *82*, 675–684.

Deng, C., Wynshaw-Boris, A., Kuo, A., Zhou, F., and Leder, P. (1996). Fibroblast growth factor receptor-3 is a negative regulator of bone growth and development. Cell *84*, 911–921.

Donehower, L.A., Harvey, M., Slagle, B.L., McArthur, M.J., Montgomery, C.A., Jr., Butel, J.S., and Bradley, A. (1992). Mice deficient for p53 are developmentally normal but susceptible to spontaneous tumors. Nature *356*, 215–221.

Dulic, V., Kauffmann, W.K., Wilson, S.J., Tisty, T.D., Lees, E., Harper, J.W., Elledge, S.J., and Reed, S.I. (1994). p53-dependent inhibition of cyclin-dependent kinase activities in human fibroblasts during radiation-induced G1 arrest. Cell *76*, 1013–1023.

Easton, D.F. (1994). Cancer risks in A-T heterozygotes. Int. J. Radiat. Biol. *66*, S177–S182.

Gatti, R.A., Berkel, I., Boder, E., Braedt, G., Charmley, P., Concannon, P., Ersoy, F., Foroud, T., Jaspers, N.G., Lange, K., Lathrop, G.M., Leppert, M., Nakamura, Y., O'Connell, P., Patterson, M., Salser, W., Sanal, O., Silver, J., Sparkes, R.S., Susi, E., Weeks, D.E., Wei, S., White, R., and Yoder, F. (1988). Localization of an ataxia-telangiectasia gene to chromosome 11q22-23. Nature *336*, 577–580.

Gilad, S., Khosravi, R., Uzeil, T., Ziv, Y., Rotman, G., Savitsky, K., Smith, S., Harnik, R., Shkedi, D., Frydman, M., Chessa, L., Sanal, O., Portnoi, S., Goldwicz, Z., Jaspers, N.G.J., Gatti, R.A., Lenoir, G., Lavin, M.F., Tatsumi, K., Wegner, R.D., Shiloh, Y., and Bar-Shira, A. (1996). Ataxia-telangiectasia: predominance of mutations that inactivate the ATM protein by truncations or large deletions. Hum. Mol. Genet. *5*, 433–439.

Gurney, M.E., Haifeng, P., Chiu, A.Y., Dal Canto, M.C., Polchow, C.Y., Alexander, D.D., Caliendo, J., Hentati, A., Kwon, Y.W., Deng, H.-X., Chen, W., Zhai, P., Sufit, R.L., and Siddique, T. (1994). Motor neuron degeneration in mice that express a human Cu,Zn superoxide dismutase mutation. Science *264*, 1772–1775.

Hallahan, D.E., Dunphy, E., Virudachalam, S., Sukatme, V.P., Kufe, D.W., and Weichselbaum, R.R. (1995). c-*jun* and *Egr-1* participate in DNA synthesis and cell survival in response to ionizing radiation exposure. J. Biol. Chem. *270*, 30303–30309.

Harlow, E., and Lane, D. (1988). Antibodies: A Laboratory Manual (Cold Spring Harbor, New York: Cold Spring Harbor Laboratory Press).

Heintz, N. (1993). Cell death and the cell cycle: a relationship between transformation and neurodegeneration? Trends Biochem. Sci. *18*, 157–159.

Heppell, A., Butterworth, S.V., Hollis, R.J., Kennaugh, A.A., Beatty, D.W., and Taylor, A.M. (1988). Breakage of the T cell receptor α chain locus in non-malignant clones from patients with ataxia telangiectasia. Hum. Genet. *79*, 360–364.

Hogan, B., Beddington, R., Costantini, F., and Lacy, E. (1994). Manipulating the Mouse Embryo: A Laboratory Manual, Second Edition (Cold Spring Harbor, New York: Cold Spring Harbor Laboratory Press).

Houldsworth, J., and Lavin, M.F. (1980). Effect of ionizing radiation on DNA synthesis in ataxia telangiectasia cells. Nucl. Acids Res. *8*, 3709–3720.

Jacks, T., Remington, L., Williams, B.O., Schmitt, E.M., Halachmi, S., Bronson, R.T., and Weinberg, R.A. (1994). Tumor spectrum analysis in p53-mutant mice. Curr. Biol. *4*, 1–7.

Johnson, R.S., van Lingen, B., Papaioannou, V.E., and Spiegelman, B.M. (1993). A null mutation at the *c-jun* locus causes embryonic lethality and retarded cell growth in culture. Genes Dev. *7*, 1309–1317.

Jung, M., Zhang, Y., Lee, S., and Dritschilo, A. (1995). Correction of radiation sensitivity in ataxia telangiectasia cells by a truncated IκB-α. Science *268*, 1619–1621.

Kastan, M.B., Zhan, Q., el-Deiry, W.S., Carrier, F., Jacks, T., Walsh, W.V., Plunkett, B.S., Vogelstein, B., and Fornace, A.J., Jr. (1992). A mammalian cell cycle checkpoint pathway utilizing p53 and GADD45 is defective in ataxia-telangiectasia. Cell *71*, 587–597.

Kato, R., and Ogawa, H. (1994). An essential gene, ESR1, is required for mitotic growth, DNA repair and meiotic recombination in *Saccharomyces cerevisiae*. Nucl. Acids Res. *22*, 3104–3112.

Kemp, C.J., Wheldon, T., and Balmain, A. (1994). p53-deficient mice are extremely susceptible to radiation-induced tumorigenesis. Nature Genet. *8*, 66–69.

Kojis, T.L., Gatti, R.A., and Sparkes, R.S. (1991). The cytogenetics of ataxia telangiectasia. Cancer Genet. Cytogenet. *56*, 143–156.

Kuerbitz, S.J., Plunkett, B.S., Walsh, W.V., and Kastan, M.B. (1992). Wild-type p53 is a cell cycle checkpoint determinant following irradiation. Proc. Natl. Acad. Sci. USA *89*, 7491–7495.

Lane, D.P. (1992). p53, guardian of the genome. Nature *358*, 15–16.

Liu, N., and Bryant, P.E. (1994). Enhanced chromosomal response of ataxia-telangiectasia cells to specific types of DNA double-strand breaks. Int. J. Radiat. Biol. *66*, S115–S121.

Livingstone, L.R., White, A., Sprouse, J., Livanos, E., Jacks, T., and Tisty, T.D. (1992). Altered cell cycle arrest and gene amplification potential accompany loss of wild-type p53. Cell *70*, 923–935.

Lowe, S.W., Schmitt, E.M., Smith, S.W., Osborne, B.A., and Jacks, T. (1993). p53 is required for radiation-induced apoptosis in mouse thymocytes. Nature *362*, 847–849.

Luna, L.G. (1992). Histopathological Methods and Color Atlas of Special Stains and Tissue (Gaithersburg, Maryland: American Histolabs, Inc. Publications Division).

Metcalfe, J.A., Heppell-Parton, A., McConville, C.M., and Taylor, A.M. (1991). Characterization of a B-lymphocyte t(2;14) (p11;q32) translocation from an ataxia telangiectasia patient conferring a proliferative advantage on cells *in vitro*. Cytogenet. Cell Genet. *56*, 91–98.

Meyn, M.S. (1995). Ataxia-telangiectasia and cellular responses to DNA damage. Cancer Res. *55*, 5991–6001.

Painter, R.B., and Young, B.R. (1980). Radiosensitivity in ataxia-telangiectasia: a new explanation. Proc. Natl. Acad. Sci. USA *77*, 7315–7317.

Pandita, T.K., and Hittelman, W.N. (1992a). The contribution of DNA and chromosome repair deficiencies to the radiosensitivity of ataxia-telangiectasia. Radiat. Res. *131*, 214–223.

Pandita, T.K., and Hittelman, W.N. (1992b). Initial chromosome damage but not DNA damage is greater in ataxia telangiectasia cells. Radiat. Res. *130*, 94–103.

Pecker, I., Avraham, K.B., Gilbert, D.J., Savitsky, K., Rotman, G., Harnik, R., Fukao, T., Schröck, E., Hirotsune, S., Tagle, D., Collins, F.S., Wynshaw-Boris, A., Ried, T., Copeland, N.G., Jenkins, N.A., Shiloh, Y., and Ziv, Y. (1996). Identification and chromosomal localization of *Atm*, the murine homolog of the ataxia-telangiectasia gene. Genomics, in press.

Powell, S., Whitaker, S., Peacock, J., and McMillan, T. (1993). Ataxia telangiectasia: an investigation of the repair defect in the cell line AT5BIVA by plasmid reconstitution. Mutat. Res. *294*, 9–20.

Purdie, C.A., Harrison, D.J., Peter, A., Dobbie, L., White, S., Howie, S.E., Salter, D.M., Bird, C.C., Wyllie, A.H., Hooper, M.L., and Clarke, A.R. (1994). Tumour incidence, spectrum and ploidy in mice with a large deletion in the p53 gene. Oncogene *9*, 603–609.

Rabbitts, P., Impey, H., Heppell-Parton, A., Langford, C., Tease, C., Lowe, N., Bailey, D., Ferguson-Smith, M., and Carter, N. (1995). Chromosome specific paints from a high resolution flow karyotype from the mouse. Nature Genet. *9*, 369–375.

Russo, G., Isobe, M., Pegoraro, L., Finan, J., Nowell, P.C., and Croce, C.M. (1988). Molecular analysis of a t(7;14)(q35;q32) chromosome translocation in a T cell leukemia of a patient with ataxia telangiectasia. Cell *53*, 137–144.

Sango, K., Yamanaka, S., Hoffmann, A., Okuda, Y., Grinberg, A., Westphal, H., McDonald, M.P., Crawley, J.N., Sandhoff, K., Suzuki, K., and Proia, R.L. (1995). Mouse models of Tay-Sachs and Sandhoff diseases differ in neurologic phenotype and ganglioside metabolism. Nature Genet. *11*, 170–176.

Savitsky, K., Bar-Shira, A., Gilad, S., Rotman, G., Ziv, Y., Vanagaite, L., Tagle, D.A., Smith, S., Uziel, T., Sfez, S., Ashjenazi, M., Pecker, I., Frydman, M., Harnik, R., Patanjali, S.R., Simmons, A., Clines, G.A., Sateil, A., Gatti, R.A., Chessa, L., Sanal, O., Lavin, M.F., Jaspers, N.G.J., Taylor, A.M.R., Arlett, C.F., Miki, T., Weissman, S.M., Lovett, M., Collins, F.S., and Shiloh, Y. (1995a). A single ataxia telangiectasia gene with a product similar to PI-3 kinase. Science *268*, 1749–1753.

Savitsky, K., Sfez, S., Tagle, D.A., Ziv, Y., Sartiel, A., Collins, F.S., Shiloh, Y., and Rotman, G. (1995b). The complete sequence of the coding region of the ATM gene reveals similarity to cell cycle regulators in different species. Hum. Mol. Genet. *4*, 2025–2032.

Schröck, E., Badger, P., Larson, D., Erdos, M., Wynshaw-Boris, A., Ried, T., and Brody, L. (1996a). The murine homolog of the human breast and ovarian cancer susceptibility gene *BRCA1* maps to mouse chromosome 11D. Human Genet. *97*, 256–259.

Schröck, E., du Manoir, S., Veldman, T., Schoell, B., Wienberg, J., Ferguson-Smith, M.A., Ning, Y., Ledbetter, D.H., Soenksen, D., Garini, Y., and Ried, T. (1996b). Multicolor spectral karyotyping of human chromosomes. Science, in press.

Sedgewick, R., and Boder, E. (1991). Ataxia-telangiectasia. In Handbook of Clinical Neurology, P. Vinken, G. Bruyn, and H. Klawans, eds. (New York: Elsevier Scientific Publishers), pp. 347–423.

Sherrington, P.D., Fisch, P., Taylor, A.M., and Rabbitts, T.H. (1994). Clonal evolution of malignant and non-malignant T cells carrying t(14;14) and t(X;14) in patients with ataxia telangiectasia. Oncogene *9*, 2377–2381.

Shiloh, Y. (1995). Ataxia-telangiectasia: closer to unraveling the mystery. Eur. J. Hum. Genet. *3*, 116–138.

Stern, M.H., Lipkowitz, S., Aurias, A., Griscelli, C., Thomas, G., and Kirsch, I.R. (1989). Inversion of chromosome 7 in ataxia telangiectasia is generated by a rearrangement between T-cell receptor β and T-cell receptor γ genes. Blood *74*, 2076–2080.

Sturtzbecher, H.-W., Donzelmann, B., Henning, W., Knippschild, U., and Buchhop, S. (1996). p53 is linked directly to homologous recombination processes via RAD51/RecA protein interaction. EMBO J. *15*, 1992–2002.

Taylor, A.M., Oxford, J.M., and Metcalfe, J.A. (1981). Spontaneous cytogenetic abnormalities in lymphocytes from thirteen patients with ataxia telangiectasia. Int. J. Cancer *27*, 311–319.

Taylor, A.M., Metcalfe, J.A., Thick, J., and Mak, Y.F. (1996). Leukemia and lymphoma in ataxia telangiectasia. Blood *87*, 423–438.

Thick, J., Sherrington, P.D., Fisch, P., Taylor, A.M., and Rabbitts, T.H. (1992). Molecular analysis of a new translocation, t(X;14)(q28;q11), in premalignancy and in leukaemia associated with ataxia telangiectasia. Genes Chromosom. Cancer *5*, 321–325.

Tsukada, T., Tomooka, Y., Takai, S., Ueda, Y., Nishikawa, S., Yagi, T., Tokunaga, T., Takeda, N., Suda, Y., Abe, S., et al. (1993). Enhanced proliferative potential in culture of cells from p53-deficient mice. Oncogene *8*, 3313–3322.

Tybulewicz, V.L., Crawford, C.E., Jackson, P.K., Bronson, R.T., and Mulligan, R.C. (1991). Neonatal lethality and lymphopenia in mice with a homozygous disruption of the c-*abl* proto-oncogene. Cell *65*, 1153–1163.

Uziel, T., Savitsky, K., Platzer, M., Ziv, Y., Helbitz, T., Nehls, M., Boehm, T., Rosenthal, A., Shiloh, Y., and Rotman, G. (1996). Genomic organization of the ATM gene. Genomics, *33*, 317–320.

Verma, I.M., Stevenson, J.K., Schwartz, E.M., Van Antwerp, D., and Miyamoto, S. (1995). Rel/NF-κB/IκB family: intimate tales of association and dissociation. Genes Dev. *9*, 2723–2735.

Yin, Y., Tainsky, M.A., Bischoff, F.Z., Strong, L.C., and Wahl, G.M. (1992). Wild-type p53 restores cell cycle control and inhibits gene amplification in cells with mutant p53 alleles. Cell *70*, 937–948.

Zakian, V.A. (1995). *ATM*-related genes: what do they tell us about functions of the human gene? Cell *82*, 685–687.